Creep and tensile behaviour of austenitic Fe–Cr–Ni stainless steels

Raluca Voicu, Jacques Lacaze, Eric Andrieu, Dominique Poquillon, Jader Furtado

Creep and tensile behaviour of austenitic Fe–Cr–Ni stainless steels

Raluca Voicu [a,*], Jacques Lacaze [a], Eric Andrieu [a], Dominique Poquillon [a], Jader Furtado [b]

[a] CIRIMAT, Université de Toulouse, 118 route de Narbonne, 31077 Toulouse Cedex 04, France
[b] Air Liquide – C.R.C.D 1, chemin de la Porte des Loges, Les Loges-en-Josas, 78354 Jouy-en-Josas Cedex, France

Corresponding author. Tel.: +33 5 62 88 56 85; fax: +33 5 62 88 56 63.
E-mail address: Raluca.Voicu@ensiacet.fr (R. Voicu).

A B S T R A C T

The control of creep behaviour during service of reformer tubes made of HP-40 austenitic stainless steels is still limited by the knowledge of creep mechanisms in these alloys. Two different HP-40 alloys modified with a low-level addition of Nb were studied. Creep tests were carried out at 980 and 1050 °C with different stress levels, in the range of 20–50 MPa, and their results were plotted in a Norton-type diagram. Also, low strain rate tensile tests were performed at temperature of 950, 980 or 1000 °C. As low strain rate tensile tests showed a plateau at nearly constant stress for a given strain rate, they could be somehow linked with creep tests. Accordingly, tensile and creep results were plotted together on a Larson–Miller (LMP) diagram. The fracture modes of tensile and creep samples were investigated and the effect of different parameters such as sample dimensions, temperature and atmosphere, was also studied.

Keywords:
High temperature creep tests
Low strain rate tensile tests
Austenitic stainless steels

1. Introduction

Centrifugally cast austenitic stainless steels such as those of the HK and HP series are widely used for manufacturing "reformer" tubes in the petrochemical industry for ammonia, methanol and hydrogen plants. The tubes have inside diameters of 60–120 mm and are 10–14 m long, they are designed for a nominal life of 100 000 h in service conditions, typically 980 °C with an internal pressure of 10–40 bar [1–4]. The present paper focuses on the mechanical properties of two as-cast 25Cr–35Ni–1Nb alloys tested under isothermal conditions (950, 980, 1000 and 1050 °C) in low strain rate tensile and creep experiments. As the principal mechanical load condition leading to failure is well recognized to be creep [5–12], a Norton-type representation has been used to plot the experimental creep data obtained during this study. Moreover, a Larson–Miller (LMP) diagram was drawn using the present creep results as well as literature data. It was found that low strain rate tensile tests could also be presented in the LMP diagram. The influence of sample orientation with respect to the tube axis was investigated as well as the effect of the environment and specimen dimensions. After testing, the specimens were examined using the scanning electron microscopy (SEM) to analyze microstructure changes and cracks distribution.

2. Materials and methods

The materials of this study were machined out of two tubes, labelled A and B, made of HP-40 alloy containing 1 wt.% Nb with nominal chemical composition given in Table 1. Fig. 1 presents optical macrographs of the cross-section of tubes A and B after etching with a solution made of 0.5 g $CuCl_2$, 8 ml HCl, 24 ml H_2O and 8 ml ethanol. It is seen that solidification of tube A (26 mm thick) results in radially orientated columnar grains on the outer part (16 mm thick) and an inner equiaxe zone (10 mm thick). Tube B (16 mm in thickness) exhibits only columnar grains. Both columnar and equiaxe grains show a dendritic structure. X-ray and SEM-EDX analyses on polished and un-etched samples were used to investigate the microstructure and phases present in the materials. The as-cast microstructure consists in an austenite dendritic matrix and a eutectic network of Nb-rich MC and Cr-rich M_7C_3 carbides.

Specimens for the mechanical tests were machined in the columnar region according to the schematic in Fig. 2. With such conditions, the primary dendrite trunks are perpendicular to the direction of the principal stress applied. At first, samples with a gage section of 2 mm^2 were used [13] then the gage section was increased to 8 mm^2. The two possible sample orientations, $B_{||}$ and $B_{\perp}$ as depicted in Fig. 2, were tested only for material B in the case of a slow strain rate tensile test. All other samples of this study were machined in the parallel orientation. Before testing, the specimens were mechanically polished (down to 3 μm diamond paste) and their dimensions were measured using an optical microscope. Tensile tests were performed at 950, 980 and 1000 °C generally in synthetic dry air (80% N_2, 20% O_2) using a MTS electromechanical machine equipped with a radiation furnace. One test was made under a mixture of 5% H_2 in Ar in order to look for any effect of environment on the creep behaviour. Creep tests were performed at 980 and 1050 °C under laboratory air and argon atmosphere on a creep testing device equipped with an ×20 balancing arm. In all cases, the heating rate to the target temperature was set to 50 K/min. Two thermocouples spot welded on the sample heads showed a

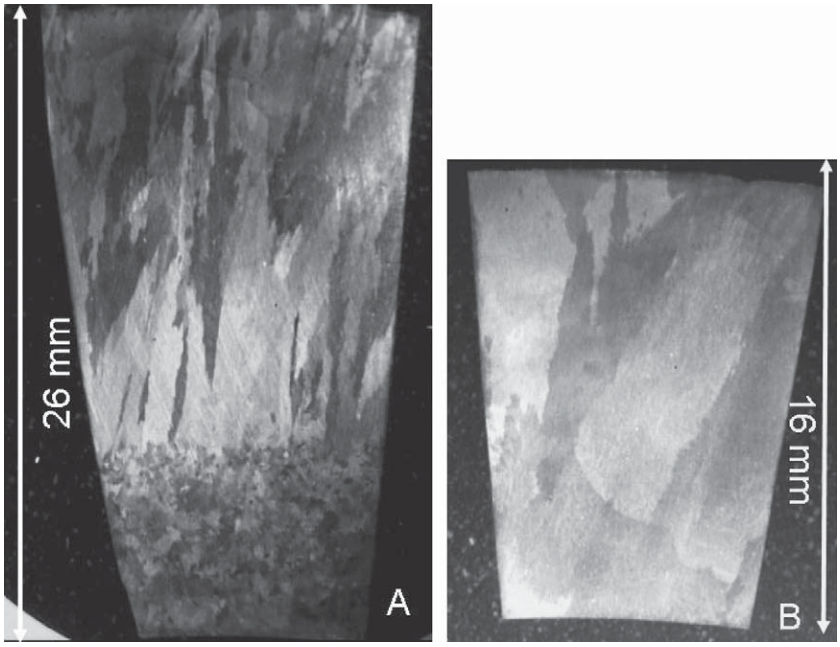

Fig. 1. Optical macrographs through the tube thickness of the two as-cast tubes, denoted A and B.

Table 1
Nominal composition (wt.%) of HP-40 alloys modified with Nb.

C	0.3–0.8
Fe	Balance
Ni	33–38
Cr	23–28
Nb	1.0
Si	1–2
Mn	1–1.5
V	<0.1
Mg	0.1

maximum temperature difference of 5 K along the 20 mm gage length. For both creep and tensile tests the deformation was measured without contact through a laser extensometer.

3. Results

The shape of the tensile curves obtained on both 2 and 8 mm^2 gage section samples showed a softening process characterized by a negative slope of the mechanical response after reaching a maximum at R_m. A typical true-stress true-strain curve highlighting this specific behaviour is presented in Fig. 3. As the maximum flow stress is reached at about 0.5% of deformation, the major part of the mechanical response is thus concerned by this softening process. The results of the tensile tests, i.e. the values of R_m and of the elongation at rupture ε_r are listed in Table 2.

It has been checked that this softening behaviour could not be related to the atmosphere used to perform the tests by comparing the results of two samples made of A material tested respectively in synthetic air and under a reducing atmosphere ($Ar + H_2$). When comparing these two tests (see Table 2), the yield stress was found to be slightly lower and the elongation at rupture slightly higher for the sample tested in reducing atmosphere than for the one tested under air. However these differences do not appear to be significant and SEM examination showed that both specimens presented similar damage after fracture. Fig. 4 illustrates that cracks have developed along the dendrites and more precisely at the interface between dendrites and eutectic carbides. The sharp decrease of the stress observed at the end of the stress–strain curves could be related to crack propagation along these interfaces. It is worth noting that the characteristic size of the dendrites, as given by the

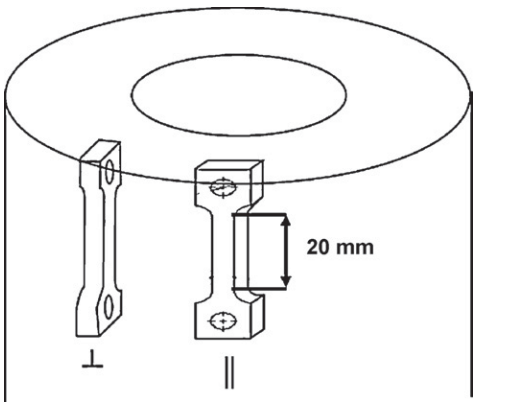

Fig. 2. Schematic showing the sampling of the specimens in the tube thickness.

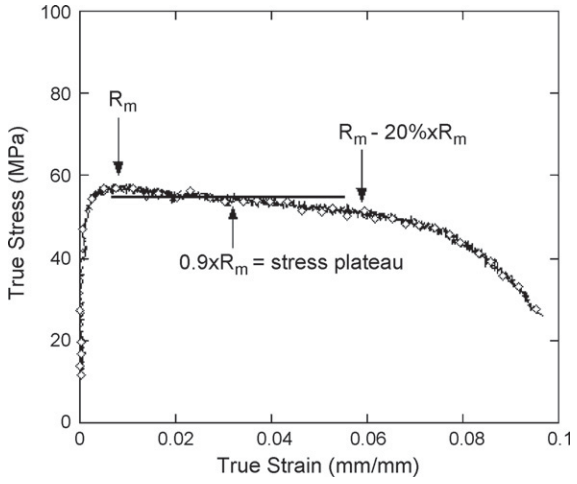

Fig. 3. Strain–stress of thin (2 mm × 1 mm) A sample after tensile test at 1000 °C; $\dot{\varepsilon} = 10^{-5}\ s^{-1}$ under reducing atmosphere (5%H_2 in Ar).

Table 2
Results of tensile tests. $\dot{\varepsilon}$ corresponds to the imposed strain rate, ε_r to the fracture strain, R_m to the maximal stress, $\sigma_{plateau}$ is defined in Fig. 3 as 0.9 R_m and the time $t_{r\ equivalent}$ corresponds to the length of the plateau, i.e. the time during which the stress decreases from R_m to 0.8 R_m. The LMP parameter was calculated using these data and the formula given in the text.

Tensile samples	Cross-section (mm^2)	Atmosphere	T (°C)	$\dot{\varepsilon}$ (s^{-1})	ε_r (%)	R_m (MPa)	$\sigma_{plateau}$ (MPa)	$t_{r\ equivalent}$ (h)	LMP
$B_{\parallel}$	2 × 1	Air	1000	10^{-5}	2.2	98	88.2	1.3	29.29
$B_{\parallel}$	2 × 1	Air	1000	10^{-5}	5.4	96	86.4	1.67	29.43
$B_{\parallel}$	2 × 1	Air	1000	10^{-5}	5.7	62	55.8	3.24	29.80
$B_{\parallel}$	2 × 4	Air	1000	10^{-5}	24	55	49.5	5.67	30.11
$B_{\perp}$	2 × 4	Air	1000	10^{-5}	18	54.5	49	5	30.04
$B_{\perp}$	2 × 4	Air	1000	10^{-3}	21	92	82.4	0.08	27.75
$A_{\parallel}$	2 × 1	Ar + 5% H_2	1000	10^{-5}	9	57.9	52.1	2.4	29.63
$A_{\parallel}$	2 × 1	Air	1000	10^{-5}	7	68	61.2	2.4	29.63
$A_{\parallel}$	2 × 1	Air	950	10^{-5}	2.8	88	79.2	0.88	27.94
$A_{\parallel}$	2 × 4	Ar	980	10^{-5}	26	57	51.3	6.6	29.72

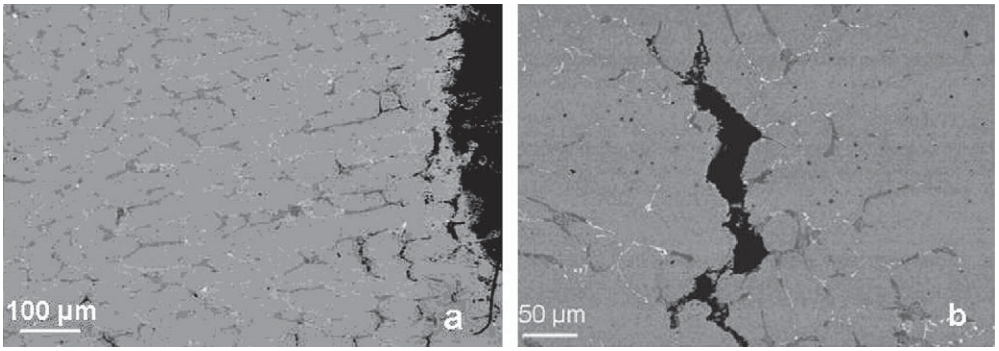

Fig. 4. (a) Low-magnification micrograph showing secondary dendrite arms; (b) Higher magnification showing a crack developed along a dendrite/eutectic interface.

average size of their secondary arms, is quite large at about 50 µm when compared to the 1-mm thickness of the samples with a 2 mm^2 gage section. It was thus decided to use larger samples (8 mm^2 gage section) than those used at the start of the study, expecting them to be large enough to consist of a representative volume of the material. As seen in Table 2, the change of the gage section led to an increase of elongation at rupture but also to a decrease of the maximum stress, though the scatter of the data is large. It may be suggested that the behaviour of both thin and thick samples is controlled, respectively, by the network of eutectic carbides and by the austenite dendrites. The thicker the section of the sample is, the higher its apparent ductility. Data in Table 2 shows also that the effect of sample orientation within the thickness of the tube turned out to be negligible. Further, the influence of the strain rate on mechanical properties has been investigated. Two B thick (8 mm^2) samples were tested at 10^{-3} and 10^{-5} s^{-1} strain rates, showing that the material has an elasto-viscoplastic behaviour [13].

As mentioned above, all the stress–strain curves obtained in slow strain rate tensile tests showed a plateau at nearly constant stress (see Fig. 3). These experiments could thus be seen as being much alike creep tests performed at the average stress of the plateau. To analyze these slow strain rate tensile tests, the duration t_r of this plateau was chosen as the period during which the stress decreases from its maximal value R_m to 0.8 R_m and the equivalent stress was set at 0.9 R_m (see Fig. 3).

Table 3 lists the characteristic data obtained from the creep tests. As for tensile tests, it is seen that the effect of the gage section could be important. Of more importance, Fig. 5 shows an example of records that illustrates the fact that the creep resistance of material B was found to be much better than the one of the material A. The micrographs associated to these curves in Fig. 6 show that coarsened intradendritic precipitates (analyzed as $M_{23}C_6$ carbides) are found in material A when very few precipitation could be evidenced in the case of material B. Note that the interdendritic eutectic M_7C_3 carbides have been fully transformed into $M_{23}C_6$ in both A and B materials during creep test, while MC carbides are stable in term of chemical composition and morphology.

Plotting the minimum creep rate versus the nominal applied stress gives the Norton diagram showed in Fig. 7. The Norton coefficient n obtained in this study is about 8, which is close to the value of 9 found by Dunlop et al. [5] on HK-40 alloy. On the Norton representation both A and B as cast materials show a slope change for stress around 30 MPa indicating that the fracture occurs because of damage developing during visco-plastic behaviour at stress value below this level. For higher stress values, plastic strain induces strain localisation rather than damage growth. This seems to be confirmed by the observation of the fractured surfaces which

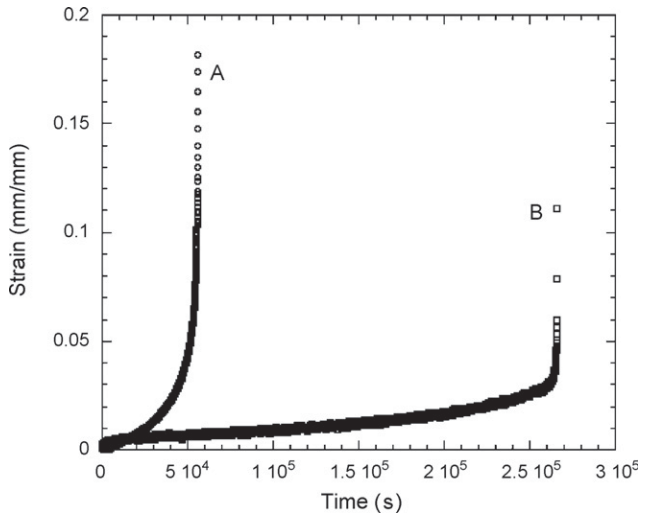

Fig. 5. Strain–time curves for A and B as-cast materials crept at 980 °C under 40 MPa in argon.

Table 3
Results of creep tests. $\dot{\varepsilon}_s$ corresponds to the minimum creep strain rate, ε_r to the fracture strain, σ to the applied creep stress, t_r to the fracture time and LMP corresponds to the Larson–Miller parameter as calculated with the formula given in the text.

Creep samples	Cross-section (mm^2)	Atmosphere	T (°C)	$\dot{\varepsilon}_s$ (s^{-1})	ε_r (%)	σ (MPa)	t_r (h)	LMP
$B_{\parallel}$	2×1	Air	1050	10^{-5}	3.8	50	0.22	29.42
$B_{\parallel}$	2×4	Ar	1050	1.3×10^{-5}	21	50	1.97	30.68
$A_{\parallel}$	2×4	Ar	1050	5×10^{-5}	23	50	0.5	29.89
$B_{\parallel}$	2×4	Ar	980	10^{-6}	15.7	50	9	29.88
$A_{\parallel}$	2×4	Ar	980	2×10^{-5}	22	50	1.4	28.87
$B_{\parallel}$	2×4	Ar	980	4×10^{-8}	11	40	73.8	31.03
$A_{\parallel}$	2×4	Ar	980	5×10^{-7}	16.8	40	15.5	30.18
$B_{\parallel}$	2×4	Ar	980	8.6×10^{-9}	>1.8	30	>388.8	–
$A_{\parallel}$	2×4	Ar	980	1.5×10^{-8}	>0.3	30	>66.6	–
$A_{\parallel}$	2×4	Ar	980	3.8×10^{-8}	17	20	146	31.4
$B_{\parallel}$	2×4	Ar	980	8×10^{-10}	>0.05	20	>49	-
$B_{\parallel}$	2×4	Ar	980	2×10^{-9}	1.8	20	833	32.35
$B_{\parallel}$	2×4	Ar	980	3×10^{-9}	>0.6	20	>611	-

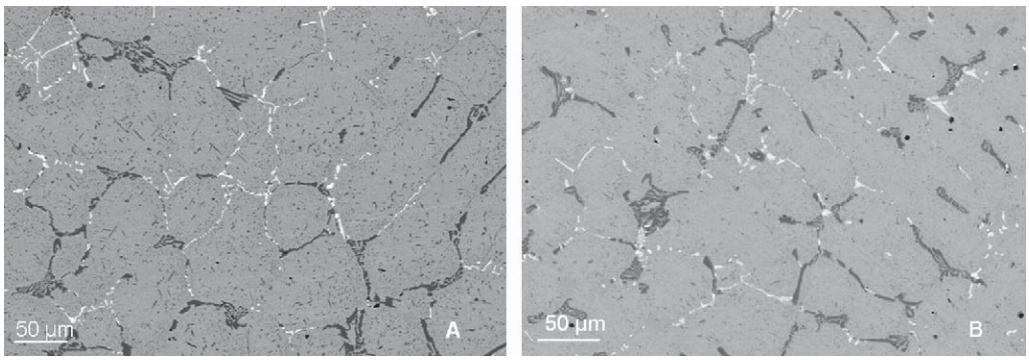

Fig. 6. Microstructures of A and B materials after creep test at 980 °C under 40 MPa in argon.

showed necking of the gage at high stress level and no necking but noticeable creep damage at low ones. Furthermore cavities located along matrix/carbides interfaces were observed on all the creep samples tested at 20 MPa.

4. Discussion

Fig. 8 shows a Larson–Miller diagram with a LMP parameter given as:

$$\mathrm{LMP} = T(22.9 + \log_{10} t_r)10^{-3},$$

where T is the temperature (in K) and t_r the time for fracture (h).

In addition to the results of the present study, data from Wu [7], Kircheiner and Woelpert [8] and Muralidharan et al. [10] have been plotted on this graph. Kirchheiner and Woelpert [8] reported a calculated creep duration of 10^5 h for HK-40 and HP-40 alloys from experiments performed between 750 °C under 40 MPa and 1100 °C under 3 MPa. Wu [7] has made experiments on HK-40 type alloys cast under different centrifugation conditions. Their creep tests were carried out at 871 °C (60, 80 and 100 MPa) and 950 °C (30, 40 and 50 MPa) and they reported their results with a different Larson Miller parameter which was thus recalculated to be plotted in Fig. 8. Muralidharan et al. [10] compared the values of t_r for two HP-40 alloys, with 1 and 2 wt.% Nb, at 982 °C (27.6 MPa) and 1093 °C (13.8 and 6.9 MPa). It is seen in Fig. 8 that the present results agree very well with the literature data, especially data obtained at low stress level. As mentioned above, the specific shape of the slow

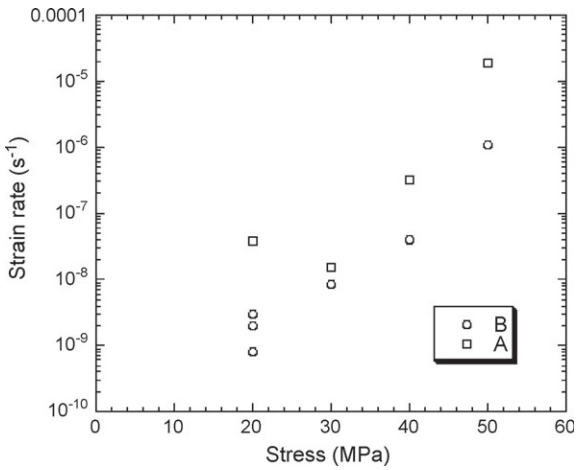

Fig. 7. Norton diagram of creep results on A and B as cast materials tested at 980 °C.

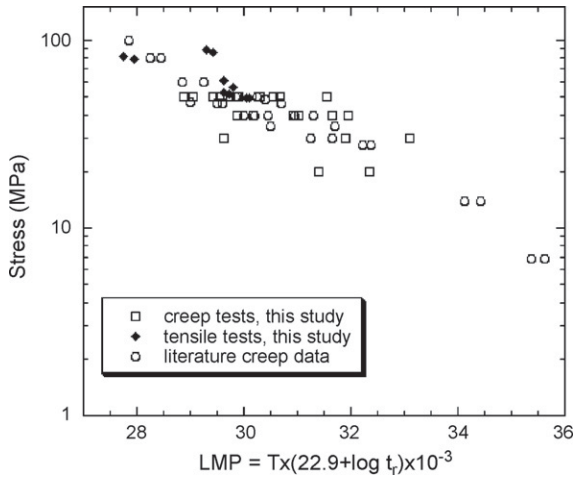

Fig. 8. Larson–Miller diagram drawn from literature creep data and tensile and creep data of this study.

strain rate tensile curves suggested considering them as creep tests made under a load $\sigma_{plateau}$ as defined in Fig. 3. The time to fracture t_r is then given by the length of the plateau. These values (Table 2) have been plotted in Fig. 8 as well. It is worth stressing that the results obtained with low strain rate tensile tests compare well with those from creep tests of this study and from literature data. This should indicate that the deformation mechanisms are not so different in creep and slow strain rate tensile tests when the stress is relatively high. In tensile tests the material shows a classical elasto-viscoplastic behaviour with positive strain rate sensitivity, the yield strength increasing with the strain rate. The strain-rate sensitivity exponent m defined as $m = \ln(\Delta\sigma)/\ln(\Delta\dot{\varepsilon})$ can be estimated using the flow stresses obtained at 10^{-3} and $10^{-5}\ s^{-1}$ (82.4 and 49 MPa, respectively, see Table 2), which gives a value of 0.11. The inverse of this value, namely 8.88, compares well with the Norton coefficient ($n = 8$) obtained in creep tests during this study and to literature work ($n = 9$) [5].

5. Conclusion

Tensile and creep tests on small samples machined out from as-cast HP-40 tubes showed a significant effect of sample dimensions. In contrast, it was found that the mechanical properties are not significantly affected by sample orientation and environment (air or reducing atmosphere). The network of MC and M_7C_3 or $M_{23}C_6$ interdendritic carbides is detrimental in slow strain rate tensile as well as in creep tests. Cracks were observed at carbides/dendrites interfaces and their propagation is likely to be responsible for the fracture of the samples. A Norton-type representation of the results showed that a change of creep mechanism from visco-plastic to plastic behaviour seems to appear at about 30 MPa. Low strain rate tensile tests showed features that led to analyze them in much the same way as creep tests at high stresses, and a Larson–Miller diagram could be drawn that includes results from both types of tests. At lower stress levels, other damage mechanisms are certainly activated during creep.

References

[1] Refineries C.o.H.-T.T.i.P, API Recommended Practice 530, 3rd ed, American Petroleum Institute, Washington, DC, 1988.
[2] I.L. May, T.L.D. Silveira, C.H. Vianna, Int. J. Pressure Vessels Piping 66 (1996) 233–241.
[3] A.K. Ray, K.S. Amarenda, N.T. Yogendra, J. Swaminathan, G. Das, S. Chaudhuri, R. Singh, Eng. Fail. Anal. 10 (2003) 351–362.
[4] M.H. Shariat, A.H. Faraji, A. Ashraf-Riahy, M.M. Alipour, Corrosion Science in the 21st Century 6 (2003) H012.
[5] G.L. Dunlop, R.J. Twigg, D.M.R. Tapplin, Scand. J. Metall. 7 (1978) 152.
[6] H. Wen-Tai, R.W.K. Honeycombe, Mater. Sci. Technol. 1 (1985) 385–389.
[7] X.Q. Wu, Mater. Sci. Eng. A293 (2000) 252–260.
[8] R. Kirchheiner, P. Woelpert, International Symposium of Niobium, 2002, pp. 1041–1054.
[9] D. Jakobi, R. Gommans, Mater. Corros. 54 (2003) 881–886.
[10] G. Muralidharan, N.D. Evans, K.C Liu, J.G. Hemrick, M.L. Santella, P.J. Maziasz, V.K. Sikka, R.I. Pankiw, Proceedings of Materials Science and Technology, edited by Iron and Steel institute and TMS, USA, 2004, pp. 651–661.
[11] K. Guan, H. Xu, Z. Wang, Nucl. Eng. Des. 235 (2005) 1447–1456.
[12] K.S. Guan, F. Xu, Z.W. Wang, H. Xu, Eng. Fail. Anal. 12 (2005) 1–12.
[13] S. Perusin, R. Peraldi, J. Lacaze, J.F. Furtado Filho, E. Andrieu, 60th Annual ABM Congress, edited by ABM, Sao Paolo, 2006, pp. 2554–2563.